DENTAL MATERIALS 35 (2019) 1360–1369

Available online at www.sciencedirect.com

ScienceDirect

journal homepage: www.intl.elsevierhealth.com/journals/dema

Effect of sintering parameters on phase evolution and strength of dental lithium silicate glass-ceramics

Ulrich Lohbauer[a], *Renan Belli*[a,*], *Alexandre Abdalla Alonso*[b], *Friedlinde Goetz-Neunhoeffer*[c], *Katrin Hurle*[c]

[a] *Friedrich-Alexander-Universität Erlangen-Nürnberg (FAU), Zahnklinik 1 – Zahnerhaltung und Parodontologie, Forschungslabor für dentale Biomaterialien, Glueckstrasse 11, 91054 Erlangen, Germany*

[b] *São Paulo State University (Unesp), Institute of Science and Technology, São José dos Campos, Brazil*

[c] *Friedrich-Alexander-Universität Erlangen-Nürnberg (FAU), GeoZentrum Nordbayern, Lehrstuhl für Mineralogie, Schlossgarten 5a, 91054 Erlangen, Germany*

ARTICLE INFO

Article history:
Received 16 April 2019
Received in revised form 5 June 2019
Accepted 8 July 2019

Keywords:
Ceramics
Materials science
Restorative materials
Crystallization
X-ray Crystallography

ABSTRACT

Objective. With the establishment of CAD/CAM technology, competing lithium silicate based formulations have been introduced for clinical use, but little is known about their phase composition. Here we investigate a commercially available SiO_2-Al_2O_3-K_2O-Li_2O-P_2O_5-ZrO_2 system to evaluate the crystal phase evolution during the second heat treatment by changing the main crystallization parameters.

Methods. With a focus on the final stage of crystallization, we characterized the dimensional changes in the crystallographic structure of the residual Li_2SiO_3 and the lithium orthophosphate (Li_3PO_4) phases with variations in crystallization parameters, i.e. time, temperature and cooling rate over the range of the glass transition temperature T_g. The phase fractions (crystalline and glass) and the sizes of coherent scattering domains (CSDs) were resolved by means of quantitative X-Ray Diffraction using Rietveld refinement combined with an external standard method (G-factor). Biaxial flexure testing was conducted to evaluate the influence of crystallization parameters on the characteristic strength and natural defect distribution.

Results. An increase in crystallization temperature from 840 to 880 °C resulted in a significant reduction of the $Li_2Si_2O_5$ content, which indicated a reversion of the Li_2SiO_3 to $Li_2Si_2O_5$ phase transformation. Reduction to 800 °C had no significant effect. Furthermore, the CSD sizes of Li_2SiO_3 and Li_3PO_4 continuously increased with increasing temperature, which was accompanied by an increase in strength parameters. Reducing the cooling rate over the range of T_g resulted in an increased strength at low failure probabilities.

Significance. These findings help to establish recommendations for adjustment of the crystallization protocol, which has potential to increase the clinical reliability of the material investigated.

* *Corresponding author at*: Research Laboratory for Dental Biomaterials, Dental Clinic 1 – Operative Dentistry and Periodontology, Glueckstrasse 11, 91054 Erlangen, Germany.
E-mail address: rbelli@dent.uni-erlangen.de (R. Belli).

https://doi.org/10.1016/j.dental.2019.07.002
0109-5641/

1. Introduction

Glass-ceramics, such as those used in prosthetic dentistry, are produced by the controlled crystallization of glasses – as opposed to spontaneous devitrification – through the manipulation of composition and thermal treatment parameters (temperature and time). Typically, a solidified glass melt containing nucleating agents (such as TiO_2, ZrO_2, P_2O_5, etc.) is heated over the glass transition temperature T_g, to promote the formation of nucleating sites during non-isothermal (increasing temperature) and/or isothermal (constant temperature) protocols [1]. By further heating, nucleation is suppressed and crystal growth is fostered, which is allowed to advance up to the desired crystal fraction by holding at higher temperatures for extended times. In dentistry, high-crystal fraction glass-ceramics are deliberately produced in a two-stage process to produce an intermediary, pre-crystallized material that is suitable for soft machining, via cooling from the nucleation temperature. The second heat-treatment (final crystallization step) is undertaken lab- or chair-side, during which the crystalline phases evolve to achieve their final size and volume fraction. These parameters determine the final mechanical properties of the glass-ceramic [2].

Lithium-silicate glass-ceramics constitute the system of choice for the two-stage crystallization process meant for usage through the CAD/CAM route, a market currently shared by two competing materials differing in their chemical composition. In their pre-crystallized state, the main crystalline phase is a nanometric lithium metasilicate (Li_2SiO_3) that is formed by heterogeneous nucleation at the interface between a disordered lithium orthophosphate (Li_3PO_4) structure and the surrounding glass [3,4]. These Li_3PO_4 "seeds" are formed just prior to Li_2SiO_3 [5]. They cannot be detected by X-ray Diffraction (XRD), but are visible by Raman Spectroscopy. In the system $72SiO_2$-$3.5Al_2O_3$-$4.0K_2O$-$12.7Li_2O$-$3.3P_2O_5$-$0.8ZrO_2$ (the numbers represent the wt.% fraction of the corresponding oxide), lithium disilicate ($Li_2Si_2O_5$) crystals begin to form at the expense of Li_2SiO_3 by reacting with SiO_2 in the 4-fold coordination ($Q^{(4)}$) at around 740 °C [6,7], and further by the reaction of Li_2O with the $Q^{(3)}$ units in the glass to result in a 60 vol.% $Li_2Si_2O_5$ and 7 vol.% Li_3PO_4 fraction material, containing no residual Li_2SiO_3 phase [8]. A slightly different crystallization kinetics takes place in the system $57SiO_2$-$2.0Al_2O_3$-$1.9K_2O$-18.3-Li_2O-$5.7P_2O_5$-$9.8ZrO_2$, where Li_2SiO_3 does not completely decompose at the usual temperature range of 740–830 °C, but perseveres in a 27 vol.% fraction in the post-crystallized material. It additionally contains 14 vol.% $Li_2Si_2O_5$ and 11 vol.% Li_3PO_4 in a ZrO_2-enriched residual glass [9]. The low SiO_2/Li_2O ratio in the latter system, together with the high amounts of ZrO_2 and P_2O_5 in the parent glass, were suggested to account for the low $Li_2Si_2O_5$ fraction and the reminiscence of unreacted Li_2SiO_3. The abundant Li_2SiO_3 phase has a high coefficient of thermal expansion [10] compared to lithium silicate-based glasses, a potential source of internal residual stresses that has been suggested to cause the appearance of cracking and high scatter in the flexural strength data [11,12].

Here we evaluate the effect of crystallization parameters of the commercial system $57SiO_2$-$2.0Al_2O_3$-$1.9K_2O$-18.3-Li_2O-$5.7P_2O_5$-$9.8ZrO_2$ by varying time, maximum temperature and the temperature to which a slow cooling rate was applied. The changes in crystalline phase fractions were calculated and the evolution of coherent scattering domains (CSD) growth was modeled using an anisotropic cuboid model for Li_2SiO_3 and Li_3PO_4. Mechanical testing was conducted to determine the dependence of flexural strength on crystallization parameters.

2. Materials and methods

2.1. Material

The dental glass-ceramic material evaluated in this study is branded Suprinity® PC and is marketed by the company Vita Zahnfabrik (Bad Säckingen, Germany) since 2013. It is advertised *as zirconia-reinforced lithium silicate* due to the addition of 8–12 wt.% ZrO_2 in the initial glass composition. In a recent Raman Spectroscopy and X-Ray Diffraction analysis [4], Suprinity® PC has been shown to contain Li_2SiO_3 and Li_3PO_4 as crystalline phases in the pre-crystallized state, which persist in the material after final crystallization treatment with an additional $Li_2Si_2O_5$ phase appearing. No crystalline ZrO_2 or other Zr-containing phases were found in both pre- and post-crystallized states, though.

2.2. Crystallization parameters

The crystallization parameters were deliberately varied from the reference program (*REF*) defined by the manufacturer, namely, a heating rate of 55 °C/min to a max. temperature of 840 °C, holding time of 8 min at max. temperature, and cooling down inside the oven until 680 °C was reached, after which the oven's lift opened down and exposed the samples to convective air at ambient temperature of 20–25 °C (Vacumat 4000, Vita Zahnfabrik, Bad Säckingen, Germany). Variations of the reference program were related to the max. crystallization temperature, holding time at max. temperature and the temperature until which the specimens were slowly cooled inside the oven. These parameters varied as follows: (i) at the max. temperature of 840 °C the holding time was either 4 min, 8 min (*REF*) or 12 min; (ii) with a holding time of 8 min, the max. temperature was either 800 °C, 840 °C (*REF*), 860 °C or 880 °C and; (iii) at a max. temperature of 840 °C for 8 min (*REF*), the temperature until which the samples remained in the oven before opening was either 680 °C (*REF*) or 550 °C, which means that in the latter case, cooling at a slow rate was performed below T_g, determined to be at 636 °C [13]. This resulted in six different experimental groups.

2.3. Analysis of phase evolution

Pre-crystallized blocks of the same batch (LOT 56800), having dimensions of approx. $14 \times 12 \times 18$ mm^3, were sectioned along their long axis to obtain rectangular plates. These plates were treated with different crystallization parameters described in the previous section.

A D8 diffractometer (Bruker AXS, Karlsruhe) equipped with a 9-fold sample changer was used for XRD analysis, with the following measurement parameters: Range 6°-70° 2θ; step size 0.011° 2θ; integration time 0.3 s; radiation: copper K_α; generator

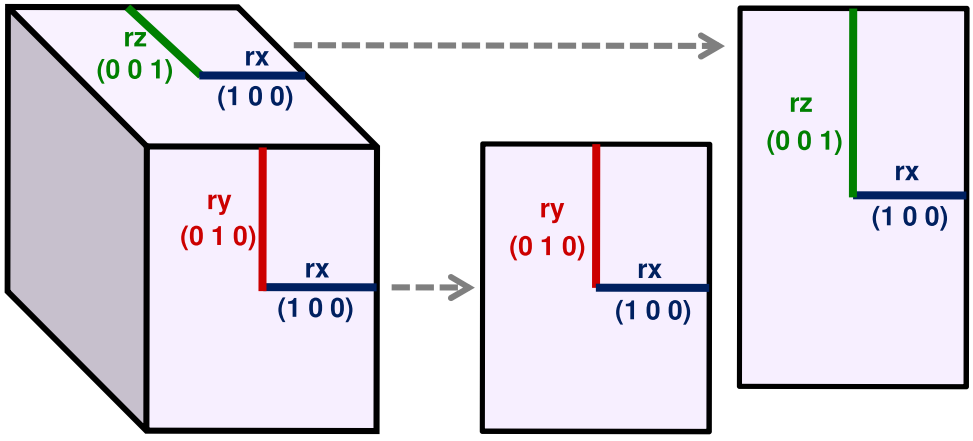

Fig. 1 – Cuboid model used for the refinement of anisotropic CSDs in Li_2SiO_3 and Li_3PO_4.

settings: 40 kV, 40 mA; divergence slit: variable V12; detector: LynxEye. Rietveld refinement was performed with software TOPAS 4.2 (Bruker AXS, Karlsruhe). The ICSD structures given in [9] were used for the refinement of the crystalline phases in addition to ICSD# 66243 for Y_2O_3 [14] while the contribution of the amorphous glass phase was fitted by a *hkl* phase derived from the structure of Li_2SiO_3. A special cuboid model for refinement of anisotropic CSD sizes was applied for Li_2SiO_3 and Li_3PO_4, where *rx* was aligned parallel to the crystallographic *a* axis, *ry* to the *b* axis and *rz* to the *c* axis for both phases (Fig. 1) [15]. The "true crystallite size" (*True CS*) was calculated as the cube root of the volume of the geometric model [16], according to Eq. (1):

$$True\,CS = \sqrt[3]{8 \cdot rx \cdot ry \cdot rz} \tag{1}$$

The absolute quantities of the crystalline phases and the residual glass in the glass ceramics was obtained by application of the G-factor method, an external standard method [17]. In this study, a quartzite slice (fine grained rock of almost pure quartz) calibrated with 100% crystalline silicon powder (NIST Si Standard 640d) was used as external standard. The G-factor was determined according to Eq. (2) [18]:

$$G = S_q \frac{\rho_q V_q^2 \mu_q^*}{c_q} \tag{2}$$

The Rietveld scale factor of quartz (S_q), the density of quartz (ρ_q) and the unit-cell volume of quartz (V_q) were obtained from Rietveld refinement of the quartz in quartzite. The mass attenuation coefficient (mac) of the quartzite (μ_q^*) was calculated from the macs of the constituting elements, which were taken from the International Tables for Crystallography [19]. The same accounts for the macs of the glass ceramic samples (μ_{sample}^*).

The absolute quantity of any crystalline phase *j* present in the sample investigated was then obtained using Eq. (3):

$$c_j = S_j \frac{\rho_j V_j^2 \mu_{sample}^*}{G} \tag{3}$$

After quantification of all crystalline phases detected in the samples according to the above described procedure, the amorphous content could be calculated as the difference of the sum of the quantified crystalline phases to 100 wt.%.

2.4. *Strength testing*

The Ball-on-Three-Balls (B3B) biaxial strength test, first introduced in Ref. [20], was conducted using an especially designed assembly [11]. The well-defined load transfer in the B3B (three point contact) allows testing of specimens with flatness deviations up to 16% [21], and small warpings present in as-sintered specimens. The influence of friction is considerably reduced when compared to fixed supports, as the loading balls roll outward during bending of the specimen [21]. Unlike rotationally symmetric set-ups (e.g., ring-on-ring), the stress field at the tensile side of the specimen has a threefold symmetry in the B3B assembly [20]. The load is transferred through a small contact area to the specimen by the central ball, with generated tensile stresses being highly dependent upon the radius of this contact area, which is, in turn, a function of the elastic moduli of the tested material and balls [20]. The thickness of the B3B specimens was measured at their center with rounded-tip digital dial gages with resolution of 0.002 mm (ID-C112XB, Mitutoyo, Japan). Support and loading balls with the same radius (R_b = 4 mm) were used. Specimens were tested in a universal testing machine (Z2.5, ZwickRoell, Ulm, Germany) at cross-head speed of 1.5 mm/min to minimize slow crack growth (fracture took place within 5–10 s). The biaxial strength was calculated using Eq. (4), as the maximum principal stress that takes place at the center top of the specimen, which scales

with the force applied F, and the inverse of the square root of the thickness t:

$$\sigma_{max} = \delta \frac{F}{t^2} \quad (4)$$

where δ is a function derived using numeric solutions for the specific assembly and specimen geometry used in this study [11], that reads:

$$\delta = f\left(\frac{t}{R_a}, \nu\right) = 0.323308 + \frac{(1.30843 + 1.44301\nu) \times \left[1.78428 - 3.15347\,(t/R_a) + 6.67919(t/R_a)^2 - 4.62603(t/R_a)^3\right]}{1 + 1.71955\,(t/R_a)} \quad (5)$$

Here ν is the Poisson's ratio of the tested material, taken from Ref. [4]. As the Poisson's ratio for the pre-crystallized material was not known, ν of the post-crystallized material was used instead as a reasonable approximation. By using rectangular plates instead of discs as specimens, the test loses the three-fold symmetry and acquires a mirror-symmetry that intersects one of the loading points. Because the extra material on the edges of plates stiffens the specimen, an important effect on the bending strain is observed, requiring a new numerical analyses for the function f. Strength obtained using the B3B test with rectangular plates has been validated extensively for alumina, silicon nitride and a capacitor ceramic in Refs. [22] and [23], where rectangular plate testing has been shown to yield values comparable to those obtained with discs described by the prediction of Weibull scaling theory. The strength data was treated using Weibull statistics and the Maximum Likelihood Estimation routine for obtaining the scale (σ_0) and shape (m) parameters corrected by the number of specimens.

3. Results

In Figs. 2–4 the radii of the cuboid models applied for the refinement of anisotropic CSDs are presented for Li_2SiO_3 and Li_3PO_4 for the [1 0 0], [0 1 0] and [0 0 1] crystallographic directions, together with the *True CS data*, for the varying crystallization parameters. Within the range of variation in sintering time and temperature analyzed here, the dimensions of the crystallites increased in a nearly linear fashion. While this effect was very clear for the temperature increase, this development was hardly significant for the sintering time. The CSD sizes of Li_3PO_4 were an exception, as they have shown to reach a plateau of growth within 8 and 12 min at 840 °C. In samples that were slowly cooled inside the oven until below T_g, a trend towards higher CSD dimensions in each crystallographic direction and *True CS* was observed compared to those rapidly cooled to 680 °C, although the differences were hardly significant. The quantitative phase composition for the different samples is given in Table 1.

The results of the biaxial strength testing are depicted in Table 2 and illustrated in Fig. 5. Compared to the reference crystallization program defined by the manufacturer, the sintering time has shown to be the most important variable influencing the characteristic strength σ_0. Decreasing the holding time by 4 min lead to a significant decrease in strength; the opposite being true for a 4 min increase in time. The temperature (20 °C higher or 40 °C lower than 840 °C) did not affect σ_0 significantly. On the other hand, a slow cooling rate below T_g showed a – barely insignificant – trend of decreasing σ_0 but increasing the strength at low failure probabilities (e.g. at clinically relevant failure levels of $P_F = 5\%$), a consequence of a significant increase in the Weibull modulus m. In contrast, the scatter in strength, illustrated by m, has shown to be consistently low (between 3 and 6) for all other groups including the pre-crystallized samples.

4. Discussion

Our strength experiments confirmed the low Weibull modulus m obtained for this lithium silicate glass-ceramic obtained in previous studies in which crystallization followed the reference program [11,12]. m-values between 3 and 6 were obtained here regardless of time and temperature variations, but most remarkably, also for the material in the pre-crystallized state. The m parameter describes the distribution of flaw sizes controlling fracture, and has been suggested in Ref. [11] to be determined, in this specific material, by the severe cracking induced by internal residual stresses. The fact that such a low m-value (unusual for modern glass-ceramics [24]) has been obtained for the pre-crystallized material suggests a flaw population of similar nature to the one observed for the post-crystallized material. In scanning electron micrographs of etched samples (see Fig. 6), we found cracking in both the pre- and the post-crystallized samples. These are natural material flaws. In a recent study [8], the use of coarse diamond grinding on both sets of samples lead to an increase in m to 12.5 for the pre-crystallized, and to 10.5 for the post-crystallized material. Coarse grinding creates a different flaw population of a narrower flaw size distribution that starts to dominate the fracture mode [8]. The critical flaw sizes for those samples were calculated to be approx. 18 μm and 14 μm, respectively. The critical flaws in our fine-ground samples in this study must be below those dimensions and have a much wider distribution in size.

By using a slower cooling rate below T_g, a significant increase in the m-value was obtained here, a clear indication that a thermal component is influencing the strength-controlling defects in the samples that follow the reference program. The cooling rate therein advocates the fast opening of the oven at 680 °C, while the material is still above the softening temperature (T_g of this material has been measured to 636 °C [13]). Fast-cooling rates from above T_g give little time for the material, while still in the viscoelastic state, to rearrange and release potential thermal stresses between the crystal and glass phases. This seems also to reflect on the crystallite dimensions as shown here, where longer relaxation times (fast-cooling first after 550 °C was reached) resulted in a slight trend of increasing crystallite CSDs (Fig. 3). Presumably, because of the relatively high coefficient of thermal expansion of Li_2SiO_3 ($15 \times 10^{-6}\,K^{-1}$ [10]), its high amount in both pre- and post-crystallization states might result in the generation

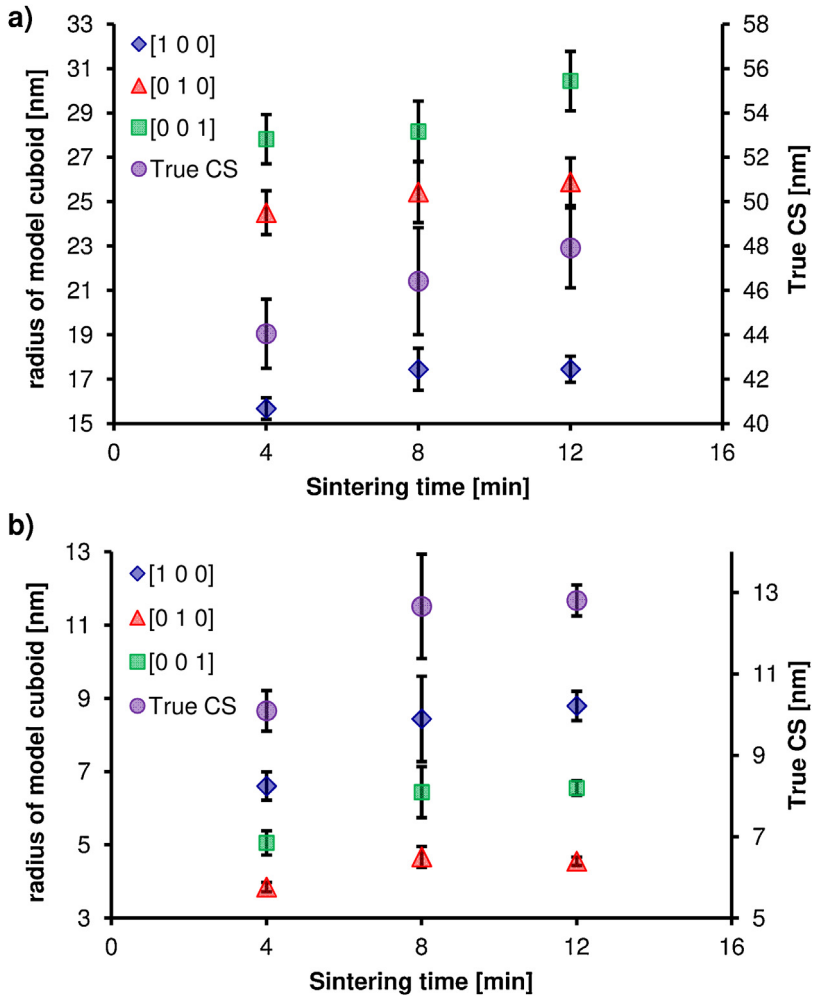

Fig. 2 – Crystallite sizes of (a) Li_2SiO_3 and (b) Li_3PO_4 in sample Suprinity® PC treated with *different sintering times*, refined with a cuboid model according to [16]; the means of the measurements of three slices out of one block are presented for each condition.

Table 1 – Quantitative phase composition of the material Suprinity® PC, treated with different sintering temperatures, times or cooling temperature; the data were obtained by G-factor quantification. The means of the measurements of three slices out of one block are presented for each condition; for the pre-crystallized sample and the REF, nine slices originating from three blocks (three slices per block) were analyzed.

Temp. [C°]	Time at Temp. [min.]	Cooling Temp. [C°]	Deviation from Reference program	Li_2SiO_3	$Li_2Si_2O_5$	Li_3PO_4	Y_2O_3	$(Y,REE)_4Al_2O_9$	Amorphous (glass)
840	8	680	Reference program	25.6 ± 0.4	13.3 ± 0.7	10.7 ± 0.3	n.d.	0.2 ± 0.1	50 ± 1
860	8	680	20 °C Increase in Temperature	26.9 ± 0.5	12.0 ± 0.3	10.7 ± 0.1	n.d.	0.16 ± 0.04	50.2 ± 0.4
880	8	680	40 °C Increase in Temperature	29.7 ± 1.0	7.10 ± 0.9	10.6 ± 0.2	n.d.	n.d.	52.6 ± 0.7
800	8	680	40 °C Decrease in Temperature	25.1 ± 0.6	13.3 ± 0.9	11.5 ± 0.2	n.d.	n.d.	50.0 ± 0.4
840	12	680	4 min. Increase in Time	25.4 ± 0.6	14.8 ± 0.2	10.9 ± 0.2	0.51 ± 0.04	n.d.	48.4 ± 0.6
840	4	680	4 min. Decrease in Time	25.6 ± 0.3	13.2 ± 0.2	10.9 ± 0.1	n.d.	n.d.	50.3 ± 0.1
840	8	550	Slow Cooling Rate below T_g	25.6 ± 0.2	13.8 ± 0.3	11.1 ± 0.3	n.d.	0.26 ± 0.04	49.1 ± 0.5
–	–	–	Pre-crystallized	42 ± 2	n.d.	n.d.	n.d.	n.d.	58 ± 2

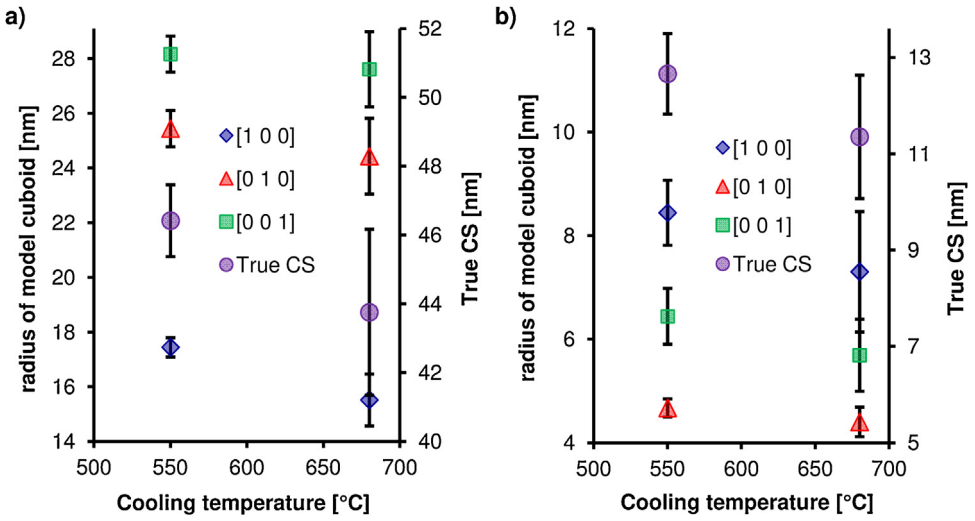

Fig. 3 – Crystallite sizes of (a) Li_2SiO_3 and (b) Li_3PO_4 in sample Suprinity® PC treated with *different cooling temperatures*, refined with a cuboid model according to [16]; the means of the measurements of three slices out of one block are presented for each condition.

Table 2 – Characteristic strength (σ_0) and strength at a clinical relevant failure probability of 5% ($\sigma_{5\%}$), Weibull modulus corrected for n = 30 (m_{corr}) and their respective 90% confidence intervals (C.I.).

Temp. [C°]	Time at Temp. [min.]	Cooling Temp. [C°]	Deviation from Reference program	m_{corr} [90% C.I.]	σ_0 [90% C.I.]	$\sigma_{5\%}$
840	8	680	Reference program	4.3 [3.4–5.4]^{a}	455.5 [424.5–489.1]^{bc}	265.7
860	8	680	20 °C increase in temperature	3.5 [2.7–4.4]^{a}	480.1 [439.7–524.4]^{ab}	216.1
880	8	680	40 °C increase in temperature	4.9 [3.9–6.1]^{a}	495.1 [466.4–522.8]^{ab}	297.9
800	8	680	40 °C decrease in temperature	3.7 [2.9–4.7] ^{a}	429.7 [395.3–467.6]^{bc}	215.5
840	12	680	4 min. increase in time	4.6 [3.7–5.9]^{a}	535.5 [501.6–572.0]^{a}	290.8
840	4	680	4 min. Decrease in time	3.1 [2.5–3.9]^{a}	331.4 [300.7–365.7]^{d}	147.3
840	8	550	Slow cooling rate below T_g	8.9 [7.0–11.0]^{b}	413.8 [399.8–428.3]^{c}	310.1
–	–	–	Pre-crystallized	4.1 [3.3–5.2]^{a}	194.5 [180.7–209.5]^{e}	83.3

Superscript letters within columns designate same statistical subsets. Groups were considered statistically indistinctive when the 90% C.I.s overlapped.

of high tensile stresses in the glass matrix. An insight on this behavior was given by fracture toughness (K_{Ic}) measurements based on the surface crack in flexure test conducted in Ref. [8]. While the pre-crystallized material of the system 72SiO_2-3.5Al_2O_3-4.0K_2O-12.7-Li_2O-3.3P_2O_5-0.8ZrO_2 (IPS e.max CAD, Ivoclar-Vivadent) has shown a K_{Ic}-value of 1.29 MPa$\sqrt{m}$ for a 34 wt.% Li_2SiO_3 fraction, the material investigated herein has shown a significantly lower K_{Ic}-value (0.91 MPa$\sqrt{m}$) despite the higher Li_2SiO_3 content (42 ± 2 wt.%). In glass-ceramics, crystal fraction goes hand-in-hand with the resistance against crack propagation (the K_{Ic} parameter) [2]. Hence, the opposite would be counter-intuitive unless some stress component of tensile nature is acting at the crack tip ($K_{c,tip}$), degrading the stress intensity factor, i.e. $K_{c,tip} = K_c - K_{res}$, with $K_{res} > 0$. Evidences of deep lateral cracks and several pop-in events during indentation, indicative of tensile stresses, have also been documented for this material [25,26]. A reduction of Li_2SiO_3 fraction from 42 ± 2 wt.% at the pre-crystallized state to 26 wt.% during crystallization leads to an increase of K_{Ic} from 0.91 MPa$\sqrt{m}$ to 1.39 MPa$\sqrt{m}$, a remarkable feat considering the modest 3.5 wt.% increase in the overall crystalline fraction. It seems compelling from these observations, that the poor mechanical performance of the evaluated material (in terms of m and K_{Ic}) is linked to the presence and amount of the Li_2SiO_3 phase.

The change in flexural strength relative to the increase or decrease in time and temperature cannot be explained solely based on the phase fraction and relative amount of crystal phases, since variations were very small. While an increase in 4 min at the maximum temperature seemed to foster the appearance of more $Li_2Si_2O_5$, an increase to 880 °C led to the reduction of the content of this phase, resulting in a difference of nearly 8 wt.% in $Li_2Si_2O_5$ and 4 wt.% in the overall crystalline fraction, which did not reflect in a significant change in σ_0. For these latter samples, the reduction of the $Li_2Si_2O_5$ content by about 6 wt.% was concomitant to the increase of the Li_2SiO_3 content in approx. 4 wt.% and 2.5 wt.% of glass fraction, indicating a reversibility in the reaction $Li_2SiO_3 + SiO_2$ ($Q^{(4)}$) ↔ $Li_2Si_2O_5$. If this was the case, it is not clear if the dissociated $Li_2Si_2O_5$ was originally formed through that route or

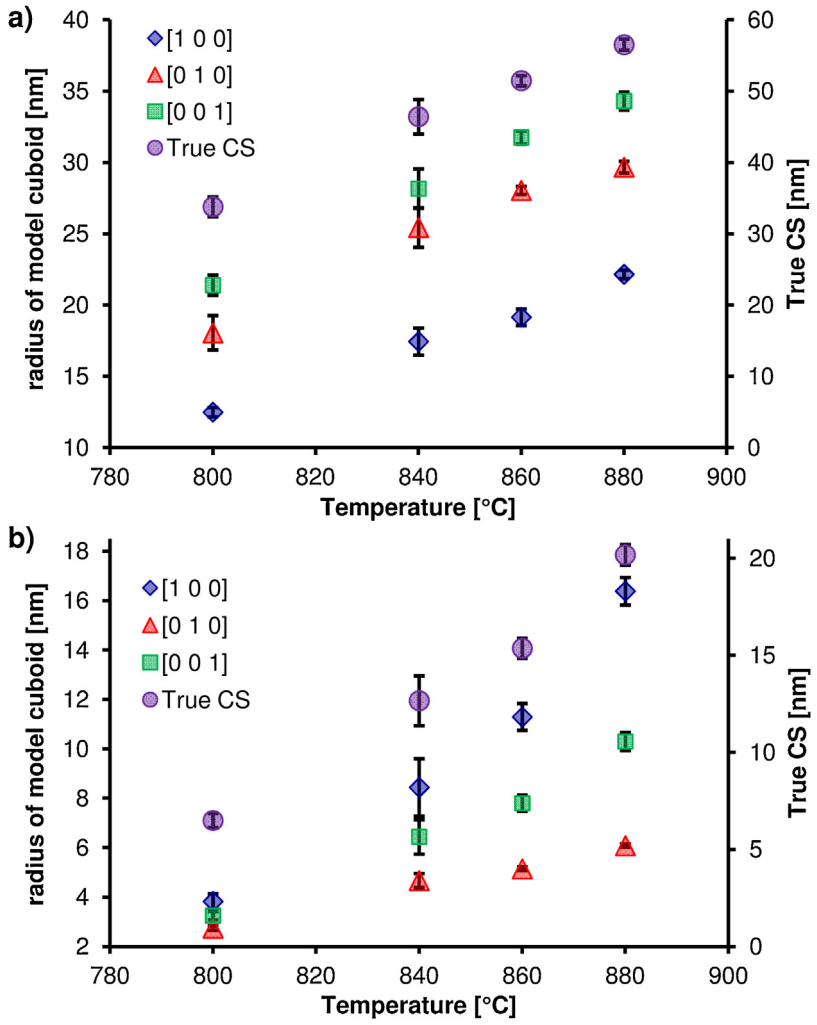

Fig. 4 – Crystallite sizes of (a) Li_2SiO_3 and (b) Li_3PO_4 in sample Suprinity® PC treated with *different sintering temperatures*, refined with a cuboid model according to [16]; the means of the measurements of three slices out of one block are presented for each condition.

by the reaction of Li_2O with two $Q^{(3)}$ units, since the latter is proposed to take place during isothermal crystallization and the former at non-isothermal conditions [7]. Alternatively, the $Li_2Si_2O_5$ phase in the samples sintered at 880 °C might have formed in shortage during the fast heating interval between 780 °C and 880 °C, to ultimately reach a temperature closer to its energy barrier for dissolution rather than further crystallization.

However, an increase in CSD dimensions, induced by increases in both time and/or temperature, lead to a consistent trend of increasing σ_0. In the case of single crystals, which are composed of only one CSD, such as the Li_2SiO_3 in this system [9], an increase in CSD might be interpreted as an increase in the crystallite size observed in the SEM. The size of second phase particulates in a matrix is known to be the single most important factor in determining K_{Ic} – a property directly correlated to strength in ceramic materials [27] – along with their aspect ratio, responsible for inducing toughening mechanisms like crack deflection and bridging [28,29]. It would be expected, therefore, that a variation in the amount of $Li_2Si_2O_5$, the phase with larger crystals here, would have had greater implications in strength than the ones observed. This was not seen, and might be rather due to the relatively small size of $Li_2Si_2O_5$ in this composition in comparison to other formulations [30–32]. Although P_2O_5 acts as a nucleating agent in SiO_2-Li_2O systems by, for example, decreasing the activation energy for Li_2SiO_3 [33], high concentrations of P_2O_5 lwere observed to mitigate the number of sites and growth rate of $Li_2Si_2O_5$ [34,35].

5. Conclusions

Crystallite dimensions of lithium metasilicate and lithium orthophosphate have shown to increase with time and temperature, while the values show a slight decrease and more scattering for faster cooling rates. An overall tendency of improved mechanical strength was observed with the increase

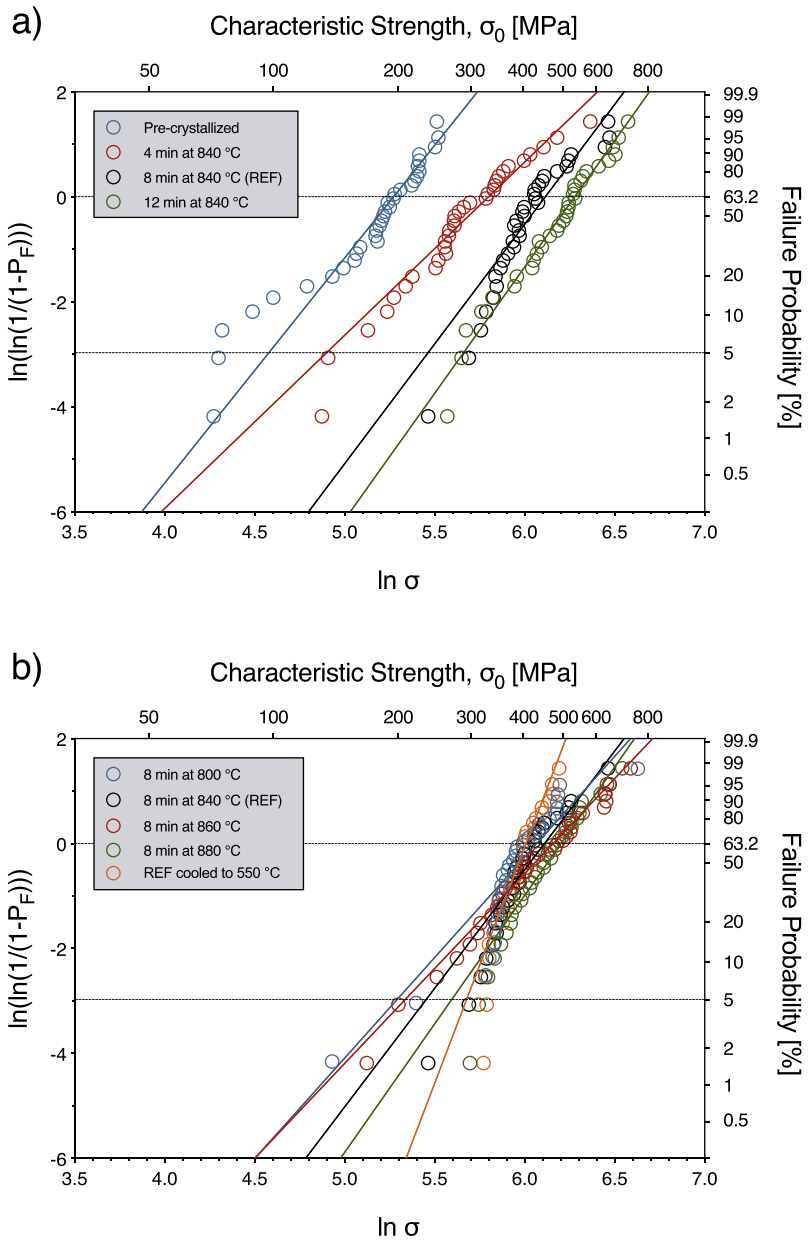

Fig. 5 – Weibull double logarithmic plot of (a) strength tests of pre-crystallized and samples crystallized with different holding times at the maximum temperature of 840 °C (all cooled slowly until 680 °C). In (b) the strength results of samples held for 8 min at different maximum temperatures (all cooled slowly until 680 °C) together with samples fired according to the Reference program from the manufacturer (REF) but cooled slowly until 550 °C).

in CSD size of Li_2SiO_3 and Li_3PO_4. A lower cooling rate showed to decrease the strength scatter significantly, contrary to the prescribed fast-cooling program that resulted in very high scatter independent of variations in time or temperature. The most significant change in crystal phase fraction was obtained by increasing the temperature to 880 °C, leading to a reversal of the metasilicate to disilicate phase transformation. To potentially increase the clinical reliability of the investigated lithium silicate glass-ceramic, an adjustment of the crystallization protocol is recommended, especially by reducing the cooling rate over the range of the glass transition temperature.

Acknowledgements

The materials tested in this study were kindly donated by the manufacturers. Author A.A.A. was supported by CAPES Foundation, Ministry of Education of Brazil, under the Process Number 88,881.132645/2016-01. The research was further partially financially supported by the Deutsche Forschungsgemeinschaft (DFG, German Research Foundation) - Grant Nr. HU 2498/1-1; GB 1/22-1.

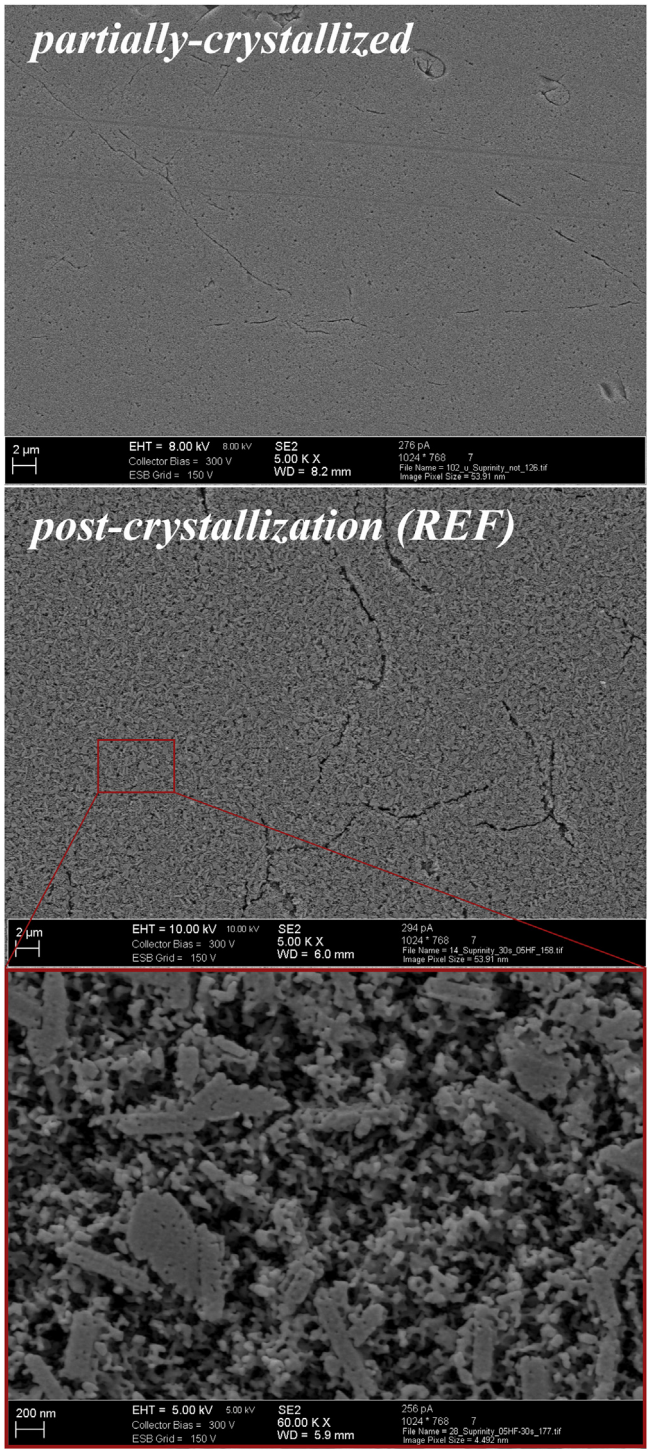

Fig. 6 – Scanning electron microscopy images of Suprinity® PC in the partially-crystallized state and after the second heat-treatment according to the REF program. Note the cracking in both states.

REFERENCES

[1] Deubener J, Allix M, Davis MJ, Duran A, Höche T, Honma T, et al. Updated definition of glass-ceramics. J Non-Cryst Solids 2018;501:3–10.

[2] Serbena FC, Mathias I, Foester CE, Zanotto ED. Crystallization toughening of a model glass-ceramic. Acta Mater 2015;86:216–28.

[3] Höland W, Beall GH. Glass-ceramic technology. second edition Hoboken, New Jersey: Wiley; 2012. p. 86.

[4] Belli R, Wendler M, de Ligny D, Cicconi MR, Petschelt A, Peterlik H, et al. Chairside CAD/CAM materials. Part 1: measurement of elastic constants and microstructural characterization. Dent Mater 2017;33(1):84–98.

[5] Chen K. Increasing the reliability of dental prosthesis by understanding crack initiation during crystallization of lithium silicate glass-ceramics. Dissertation Friedrich-Alexander-Universität Erlangen-Nürnberg; 2017.

[6] Holand W, Apel E, van't Hoen C, Rheinberger V. Studies of crystal phase formations in high-strength lithium disilicate glass-ceramics. J Non-Cryst Solids 2006;352(38–39):4041–50.

[7] Huang S, Cao P, Li Y, Huang Z, Gao W. Nucleation and crystallization kinetics of a multicomponent lithium disilicate glass by in situ and real-time Synchrotron X-ray diffraction. Cryst Growth Des 2013;13:4031–8.

[8] Belli R, Lohbauer U, Götz-Neunhoffer F, Hurle K. Crack-healing during two-stage crystallization of biomedical lithium silicate glass-ceramics. Dent Mater 2019;35:1130–45.

[9] Hurle K, Belli R, Götz-Neunhoeffer F, Lohbauer U. Phase characterization during two-stage crystallization process of lithium silicate biomedical glass-ceramics. J Non-Cryst Solids 2018;510:42–50.

[10] Santos GG, Serbena FC, Fokin VM, Zanotto ED. Microstructure and mechanical properties of nucleant-free Li2O-CaO-SiO2 glass-ceramics. Acta Mater 2017;130:347–60.

[11] Wendler M, Belli R, Petschelt A, Mevec D, Harrer W, Lube T, et al. Chairside CAD/CAM materials. Part 2: flexural strength testing. Dent Mater 2017;33(1):99–109.

[12] Riquieri H, Monteiro JB, Viegas DC, Campos TMB, de Melo RM, Saavedra GdFA. Impact of crystallization firing process on the microstructure and flexural strength of zirconia-reinforced lithium silicate glass-ceramics. Dent Mater 2018;34:1483–91.

[13] Lohbauer U, Belli R, Wendler M. Fractographic analysis of lithiumsilicate crown failures during sintering. SAGE Open Med Case Rep 2017;5:1–9.

[14] Smrock L, Duris P. Rietveld refinement of Y_2O_3 - comparison of two profile functions. In: Hasek J, editor. X-ray and neutron structure analysis in materials science. Boston, MA: Springer; 1989.

[15] Ectors D, Goetz-Neunhoeffer F, Neubauer J. A generalized geometric approach to anisotropic peak broadening due to domain morphology. J Appl Cryst 2015;48:189–94.

[16] Ectors D. Advances in the analysis of cementitious reactions and hydrate phases. Friedrich-Alexander-Universität Erlangen-Nürnberg, Dissertation; 2016.

[17] Jansen D, Stabler C, Goetz-Neunhoeffer F, Dittrich S, Neubauer J. Does ordinary portland cement contain amorphous phase? A quantitative study using an external standard method. Powder Diffr 2011;26(1):31–8.

[18] Jansen D, Goetz-Neunhoeffer F, Lothenbach B, Neubauer J. The early hydration of Ordinary Portland Cement (OPC): an approach comparing measured heat flow with calculated heat flow from QXRD. Cem Concr Res 2012;42(1):134–8.
[19] P.E. Internationall Union for Crystallography. International tables for crystallography, volume C, mathematical physical and chemical tables. third edition Wiley; 2004.
[20] Börger A, Supancic P, Danzer R. The ball on three balls test for strength testing of brittle discs: stress distribution in the disc. J Eur Ceram Soc 2002;22(9–10):1425–36.
[21] Börger A, Supancic P, Danzer R. The ball on three balls test for strength testing of brittle discs: part II: analysis of possible errors in the strength determination. J Eur Ceram Soc 2004;24(10–11):2917–28.
[22] Danzer R, Supancic P, Harrer W. Biaxial tensile strength test for brittle rectangular plates. J Eur Ceram Soc Jpn 2006;114(1335):1054–60.
[23] Harrer W, Danzer R, Supancic P, Lube T. The ball on three balls test: strength testing of specimens of different sizes and geometries. In: Proceeding of 10th ECerS Conference; 2007. p. 1271–5.
[24] Danzer R, Lube T, Supancic P, Damani R. Fracture of ceramics. Adv Eng Mater 2008;10(4):275–98.
[25] Belli R, Wendler M, Petschelt A, Lube T, Lohbauer U. Fracture toughness testing of biomedical ceramic-based materials using beams, plates and discs. J Eur Ceram Soc 2018;38(16):5533–44.
[26] Belli R, Wendler M, Zorzin JI, Lohbauer U. Practical and theoretical considerations on the fracture toughness testing of dental restorative materials. Dent Mater 2018;34(1):97–119.
[27] Ritchie RO. The conflicts between strength and toughness. Nature Mater 2011;10(11):817–22.
[28] Foulk III JW, Cannon RM, Johnson GC, Klein PA, Ritchie RO. A micromechanical basis for partitioning the evolution of grain bridging in brittle materials. J Mech Phys Solids 2007;55:719–43.
[29] Foulk III JW, Johnson GC, Klein PA, Ritchie RO. On the toughening of brittle materials by grain bridging: promoting intergranular fracture through grain angle, strength and toughness. J Mech Phys Solids 2008;56:2381–400.
[30] Dittmer M, Ritzberger C, Schweiger M, Rheinberger V, Worle M, Holand W. Phase and microstructure formation and their influence on the strength of two types of glass-ceramics. J Non-Cryst Solids 2014;384:55–60.
[31] Höland W, Apel E, van't Hoen C, Rheinberger V. Studies of crystal phase formation in high-strength lithium disilicate glass-ceramics. J Non-Cryst Solids 2006;352(S2006):4041–50.
[32] Ritzberger C, Schweiger M, Holand W. Principles of crystal phase formation in Ivoclar Vivadent glass-ceramics for dental restorations. J Non-Cryst Solids 2016;432:137–42.
[33] Gaddam A, Fernandes HR, Tulyaganov DU, Ribeiro MJ, Ferreira JMF. The roles of P2O5 and SiO2/Li2O ratio on the network structure and crystallization kinetics of non-stoichiometric lithium disilicate based glasses. J Non-Cryst Solids 2018;481:512–21.
[34] von Clausbruch SC, Schweiger M, Holand W, Rheinberger V. The effect of P2O5 on the crystallization and microstructure of glass-ceramics in the SiO2-Li2O-K2O-ZnO-P2O5 system. J Non-Cryst Solids 2000;263(1–4):388–94.
[35] Wen G, Zheng X, Song L. Effects of P2O5 and sintering temperature on microstructure and mechanical properties of lithium disilicate glass-ceramics. Acta Mater 2007;55(10):3583–91.